Tailoring the Porosity of Chemically Activated Hydrothermal Carbons: Influence of the Precursor and Hydrothermal Carbonization Temperature

Camilo Falco[1], *J.P. Marco-Lozar*[2], *D. Salinas-Torres*[2], *E.Morallón*[2], *D. Cazorla-Amorós*[2], *M.M.Titirici*[3], *D. Lozano Castello*[2]*

[1]Institute for Advanced Sustainability Studies, Berliner str 130, D-14467, Potsdam, Germany

[2]Instituto Universitario de Materiales, Universidad de Alicante. Ap. 99, E-03080 Alicante, Spain.

[3]Queen Mary University of London, School of Materials Science and Engineering, Mile End Road, E14NS, London

*Corresponding author, Fax: +34965903454, E-mail: d.lozano@ua.es (D.Lozano-Castelló).

ABSTRACT

Advanced porous materials with tailored porosity (extremely high development of microporosity together with a narrow micropore size distribution (MPSD)) are required in energy and environmental related applications. Lignocellulosic biomass derived HTC carbons are good precursors for the synthesis of activated carbons (ACs) via KOH chemical activation. However, more research is needed in order to tailor the microporosity for those specific applications. In the present work, the influence of the precursor and HTC temperature on the porous properties of the resulting ACs is analyzed, remarking that, regardless of the precursor, highly microporous ACs could be generated. The HTC temperature was found to be an extremely influential parameter affecting the porosity development and the MPSD of the ACs. Tuning of the MPSD of the ACs was achived by modification of the HTC temperature. Promising preliminary results in gas storage (i.e. CO_2 capture and high pressure CH_4 storage) were obtained with these materials, showing the effectiveness of this synthesis strategy in converting a low value lignocellulosic biomass into a functional carbon material with high performance in gas storage applications.

1. Introduction

Hydrothermal Carbonization (HTC) is now a well-established thermochemical synthesis alternative to produce functional carbon materials with a tunable chemical structure from pure carbohydrates or lignocellulosic biomass [1-3].

During HTC, biomass-derived precursors are converted into valuable carbon materials using water as reaction medium at mild temperatures (< 200°C) under self-generated pressures [4]. Even though this methodology has been known for almost 100 years [5], its full

potential, as a synthetic route for carbon materials having important applications in several fields such as catalysis, energy storage, CO_2 sequestration, water purification, soil remediation, has been revealed only recently, mainly *via* the work of Dr. Titirici and co-workers [6].

Under hydrothermal conditions monosaccharides are dehydrated to 5-hydroxymethylfurfural (5-HMF) via the well- known Lobry de Bruyn-Alberta van Ekstein rearrangement [7]. Once 5-HMF is formed, it is *in situ* "polymerised" yielding the HTC carbon product [8]. While most of the research efforts focus on the exploitation of HMF for the production of chemicals, bioplastics and biofuels [9], the Titirici´s group rediscovered these processes for the production of green and valuable carbon and carbon-hybrid materials [1,4].

One of the main limiting factors, hindering the effective and straightforward exploitation of HTC carbons for several end-applications (eg. catalysis, separation science, energy production and storage), is their low surface area and porosity [10]. In the case of monosaccharide derived HTC carbons, this problem has been elegantly overcome by using hard\soft-templating strategies or by addition of structural directing agents [11-13]. Such synthetic routes are effective because of the homogeneous nature of the pre-HTC aqueous reaction mixture. On the other hand, in the case of cellulose and more generally of lignocellulosic biomass, the same synthetic approaches are not feasible because of the insolubility of the cellulosic substrate in water. As a consequence, in order to introduce porosity in the lignocellulosic biomass derived HTC carbons, post-synthesis methods are required.

Physical or chemical activation processes are well-known strategies to produce highly porous carbons from coal-derived precursors and it has been largely described in the literature [14-20]. Their application to lignocellulosic biomass is widely used, but it is not as effective because of poor yields and low porosity development, arising from the excessive degradation

of the organic substrate [21-23]. In this regard the HTC treated biomass is characterised by a more "coal-like" chemical structure, as a consequence it may represent a more suitable precursor for the production of highly porous activated carbons (ACs).

Chemical activation of hydrothermal carbons has been previously investigated. Sevilla et al. were the first to report on the chemical activation of HTC materials as a way to generate highly porous materials. They applied the procedure to HTC materials derived from glucose, starch, furfural, cellulose and eucalyptus sawdust achieving large apparent surface areas, up to ~ 3000 m^2 g^{-1}, and pore volumes in the 0.6-1.4 cm^3 g^{-1} range. Those materials are further characterized by narrow micropore size distributions in the supermicropore range (0.7-2 nm). Tuning of the PSD was achieved through the modification of the activation temperature (600-850ºC) and the amount of KOH used (KOH/HTC weight ratio = 2 or 4). Applications of these microporous materials for supercapacitors [24], hydrogen storage [25] and CO_2 capture [26] have been reported.

Titirici and Zhao also prepared nitrogen doped activated carbon from hydrothermal carbons obtained from nitrogen containing precursors using the KOH procedure [27]. These materials were successfully used as electrodes in supercapacitors [28].

Zhang et al prepared activated carbon-based carbon/carbonaceous composites with different surface functional groups by a hydrothermal carbonization-deposition method in which commercial activated carbon was exposed to a gaseous mixture of furfural/water or furfural/acrylic acid/water at 180°C to form the carbon/carbonaceous composites. Different functional groups can be anchored onto the composite, and composites with surface hydroxyl or carboxylic or amine groups were prepared [29].

Carbonaceous monoliths rich in surface sulfonic acid groups were synthesized by one-pot hydrothermal carbonization of the mixture of p-toluene sulfonic acid/glucose/resorcinol at 180°C and further carbonized and activated to form monolithic carbons with high surface area and large pore volume. The surface area and pore volume per mass increased with prolonging

the activation time (0-6 h) and the best results on 6 h activated samples were 2337 m^2 g^{-1} and 2.12 cm^3 g^{-1}[30].

Roman et al have recently investigated the hydrothermal carbonization of various lignocellulosic biomass (walnut shell, sunflower stem and olive stone) as a more energy-efficient approach as compared with the traditional pyrolysis. The authors discovered that the final yield is higher and the initial hydrothermal treatment allows a better control over the resulting porosity [31].

However, none of these previous works investigated in detail the effect and influence of the precursor and hydrothermal carbonization temperature on the porous properties of the resulting ACs. Tuning the microporosity of the ACs is important for some energy and environmental related applications (e.g. natural gas and hydrogen storage, supercapacitors, Volatil Organic Compunds (VOC) removal), where advanced porous materials with tailored porosity (extremely high development of microporosity together with a narrow micropore size distribution (MPSD)) are required. Thus, more research is needed in HTC in order to tailor the microporosity for those specific applications.

In this manuscript, the KOH activation of HTC carbons obtained from a pure monosaccharide (i.e. glucose), its polymer (i.e. cellulose) and a real lignocellulosic biomass (i.e. rye straw) using different HTC temperatures is investigated as a function of their chemical structure. A thorough characterization of the developed porosity of these materials using both N_2 (-196 ºC) and CO_2 (0ºC) adsorption was carried out. The HTC temperature was found to be an extremely influential parameter affecting the porosity development and the MPSD of the ACs. Tuning of the MPSD of the ACs was achived by modification of the HTC temperature. Promising preliminary results in relation to the use of the chemically activated HTC carbons in gas storage (i.e. CO_2 capture and high pressure CH_4 storage) are also presented, showing the effectiveness of this synthesis strategy in converting a low value

lignocellulosic biomass (rye straw) into a functional carbon material with high performance in gas storage applications.

2. Experimental

2.1. Synthesis of the HTC carbons

10 wt% biomass (i.e. D-glucose, cellulose, rye straw) in water solutions (20 ml) were prepared and stirred overnight. The raw rye straw was grinded to a maximum particle size of 0.8 mm prior being mixed. The prepared solutions were then poured into quartz vials, subsequently placed into 50ml Teflon lined stainless steel autoclaves. The autoclaves were then heated into a programmable oven, which had been pre-heated at the desired reaction temperature. The autoclaves were cooled down in a water bath to room temperature. The HTC carbon was recovered by filtration, repeatedly washed with distilled water until the attainment of a colourless aqueous phase and finally dried at 80 ºC under vacuum overnight.

2.2. Synthesis of ACs

Chemical activation with KOH of the hydrochars were carried out using the following procedure: Physical mixtures of around 2 g of sample with corresponding amounts of KOH pellets were prepared using a hydroxide/precursor ratio of 3/1 (weight terms). The mixture was heated up to 750ºC during 2 hour under nitrogen atmosphere (500 ml min^{-1} N_2 flow rate). After such heat treatment activation, the samples were washed sequentially with HCl 5 M and distilled water and finally dried at 110ºC overnight.

2.3. Characterization

Elemental chemical analysis was performed on a (C, N, O, S, H) Vario Elmer-Perkin elemental analyzer. SEM was performed using a Gemini Leo-1550 instrument. Before imaging, material was loaded onto carbon tapes and sputtered with Au.

Porous texture characterization of the KOH-activated materials was performed by physical adsorption of N_2 at -196 ºC and CO_2 at 0ºC, using an automatic adsorption system (Autosorb-6, Quantachrome). Prior to measurements samples were degassed at 250ºC for 6 h. The relative pressure range, employed for BET surface area estimation, was chosen according to the conditions explained in the literature [32], which have been shown to yield reliable results also for highly microporous materials. The total micropore volume (V_{N2-DR}) has been determined by application of de Dubinin-Radushkevich (DR) equation to the N_2 adsorption isotherm at -196 ºC (V_{N2-DR}). V_{N2-EX} (calculated from the experimental isotherm at a relative pressure of 0.975) is the total pore volume accessible to N_2 at the measured conditions. To characterize the volume of narrow micropores (size smaller than 0.7 nm), CO_2 adsorption at 0ºC should be used, because as explained elsewhere [33-35], when nitrogen adsorption at -196 ºC is used for the characterization of microporous solids, diffusional problems of the molecules inside the narrow porosity can occur. Thus, the volume of narrow micropores (size <0.7 nm) (V_{CO2-DR}) has been calculated by application of de DR equation to the CO_2 adsorption isotherm at 0ºC [33-35].

Density of the powder activated hydrochars was determined in two different ways [36]: (i) filling a container with the activated carbon and vibrating (tap density); (ii) pressing a given amount of activated carbon in a mould at a pressure of 550 kg cm^{-2} (packing density). The amount of sample used for both type of measurements was 0.5 g approximately.

2.4. High Pressure CO_2 and CH_4 Storage Measurements

The storage of two different gases (i.e. methane and carbon dioxide) was carried out at 25 ºC using the fully automated volumetric Quantachrome device iSorbHP1 up to a pressure of

40 and 30 bar for methane and carbon dioxide, respectively. In the particular case of CO_2, also adsorption studies at 0ºC were performed for comparison purposes using the same device. In all the cases, about 300 mg of sample were placed in the analysis cell and degassed *"in situ"* at 150 ºC under vacuum for 4h. The device tests regularly for leaks. The void volume of the sample cell is determined with helium gas before each measurement. The manifold temperature was maintained at 40 ºC, while the sample volume temperature was controlled by a thermostat with cooling liquid at the analysis temperature within accuracy of ±0.02 ºC.

3. Results and Discussion

3.1. KOH chemical activation of HTC carbons.

In this section the relationship between the chemical structure of HTC carbons and their KOH chemical activation is investigated. For the purpose of this investigation, HTC carbons derived from glucose, cellulose and rye straw were synthesised at different HTC temperatures (sample names *x-y*, *x* is the initial of the carbon precursor and *y* the HTC temperature) and then activated at the same processing conditions (see experimental section). The complete porosity analysis is presented for all the materiales after the KOH activation.

3.1.1. Elemental analysis and scanning electron microscopy of ACs

The elemental composition of the HTC carbons derived ACs is characterised by very similar values regardless of the different precursors or HTC synthesis conditions (Table 1).

Table 1: EA of HTC carbon derived ACs and pyrolysed HTC carbon

	Elemental Composition (wt%)			
Sample	**C%**	**H%**	**O%**	**N%**
HTC carbon derived ACs[(a)]	85.0-88.0	1.5-2.1	10.1-12.8	0.1-0.4
HTC-Δ750[(b)]	94.0	1.7	4.2	0.1

[(a)] The EA of each AC can be found in the supporting information (Table S1)
[(b)] HTC carbon pyrolysed at 750 ºC

On the other hand, compared to HTC carbons pyrolysed at comparable temperatures (HTC-Δ750), their oxygen content is higher. This difference can be attributed to the higher degree of surface oxidation, which is typically observed after KOH chemical activation. Several oxygen-containing functional groups (eg. lactone, phenol, quinone) are known to be present on the surface of ACs [37].

SEM was used to investigate the morphology of ACs derived from glucose, cellulose and rye straw HTC carbons (Fig.1b, Fig. 1d and Fig.1f). It is evident that for all three precursors the KOH chemical activation leads to a complete morphological change. The spherical micrometer-sized particles, characterizing both glucose and cellulose derived HTC carbons (Fig. 1a and Fig. 1c) or the rye straw fibres-like structures (Fig. 1e), which are still present after HTC treatment, are not observed anymore. The ACs materials are now composed of macrometer-sized monolithic fragments with sharp edges.

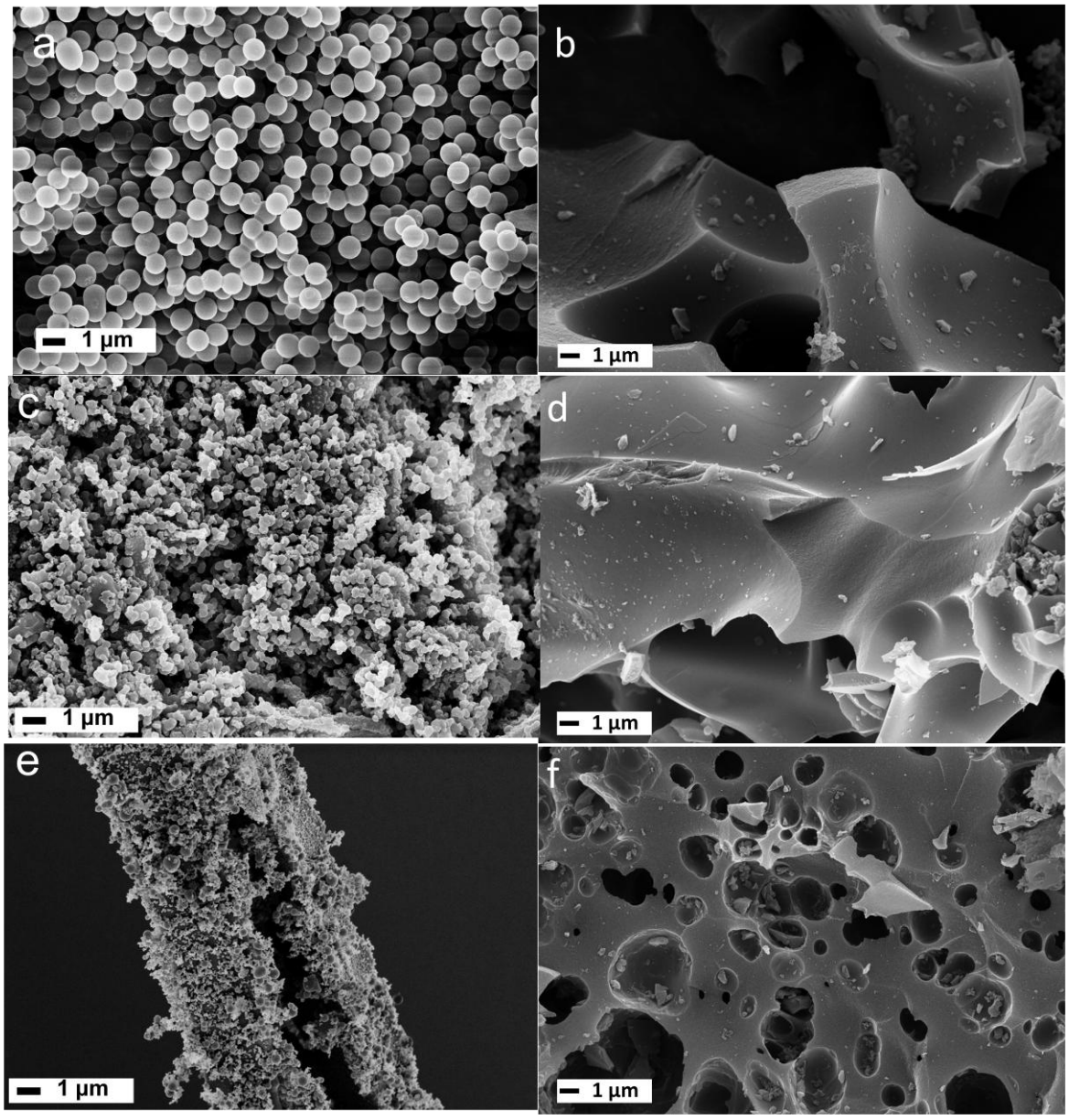

Figure 1: SEM micrographs of the hydrothermal carbon before chemical activation: (a) HTC from glucose at 240°C; (b) HTC from cellulose at 240°C; (c) HTC from rye straw at 240°C. And after chemical activation: b) glucose (G–240ºC), d) cellulose (C–240ºC) and f) rye straw (RS–240ºC).

3.1.2. Porosity analysis of ACs produced from glucose derived HTC carbon

In order to fully characterise the porosity of microporous materials, it is recommendable to employ both CO_2 and N_2 gas adsorption and to validate the obtained results by analysing them

with different theories. For this reason, an analysis based on the combination of the BET, DR and DFT models applied to N_2 and CO_2 isotherms is developed in this section.

All the N_2 isotherms of the ACs, produced from glucose derived HTC carbons, are characterised by a Type I profile (Fig. 2a). A more attentive analysis reveals that G-240^{o}C has the largest N_2 uptake, arising from a higher porosity development than in the cases of G-180^{o}C and G-280^{o}C (see apparent BET surface area and pore volumes obtained from N_2 adsorption data for these samples in Table 2). Furthermore, interestingly G-280^{o}C N_2 isotherm shows a much sharper knee at low relative pressure than G-180^{o}C and G-240^{o}C. This finding suggests that the pore size distribution (PSD) of this former sample is much narrower than for the two latter ones. Therefore, it can be deduced that G-180^{o}C and G-240^{o}C have a higher tendency to develop larger pores during chemical activation than G-280^{o}C. This conclusion is in good agreement with the QSDFT-PSD (Fig. 2b), where it is clearly seen that the sample with the narrowest PSD is G-280^{o}C, while samples G-180^{o}C and G-240^{o}C present larger contribution of wider pores.

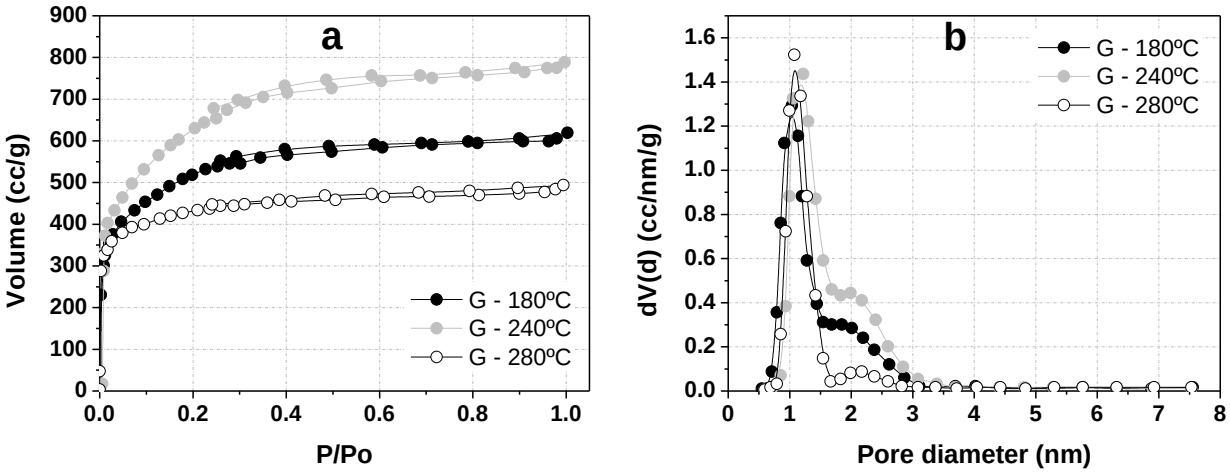

Figure 2: a) N_2 adsorption isotherms, b) N_2 adsorption QSDFT PSD of ACs (G-180^{o}C, G-240^{o}C, G-280^{o}C)

In order to assess the pore volume and the PSD of the narrow microporosity region characterising G-180^{o}C,G-240^{o}C and G-280^{o}C, CO_2 adsorption was used, since N_2 sorption is

not as effective in probing this pore range. Figure 3a presents the CO_2 adsorption isotherms (0ºC) at subatmospheric pressure and Table 2 contains also the narrow micropore volume calculated from CO_2 isotherms by applying the DR equation ($V_{CO2\text{-}DR}$). It is seen that sample G-280ºC has the largest volume of narrow microporosity, followed by G-240ºC and then G-180ºC. This trend differs from the one observed in N_2 adsorption.

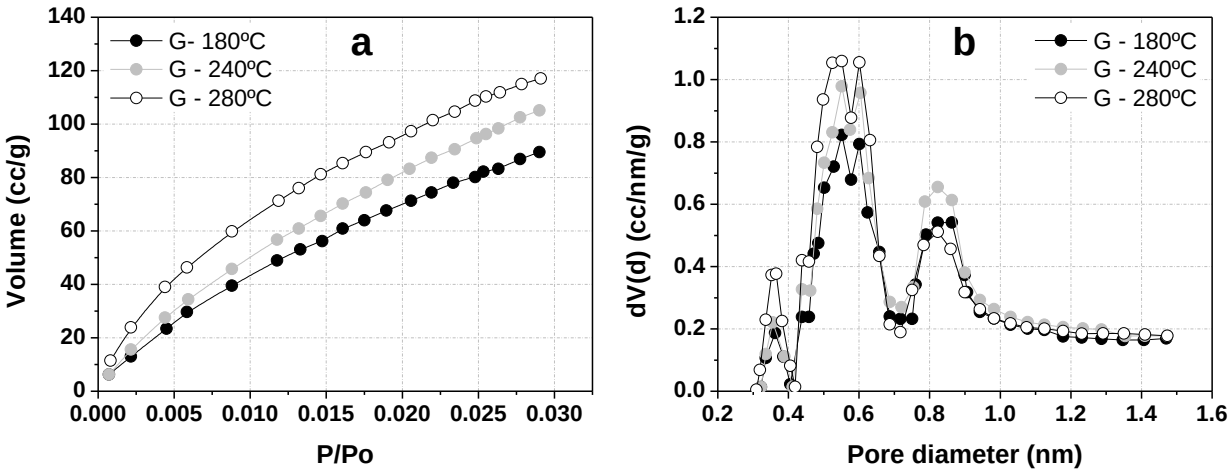

Figure 3: a) CO_2 (0ºC) isotherms and b) NLDFT PSD of ACs (G-180ºC, G-240ºC, G-280ºC)

Table 2: Calculated surface area (S) and pore volume (V) using different theories (subscript) on either N_2 or CO_2 isotherms for G-180ºC, G-240ºC, G-280ºC

Sample	$S_{N2\text{-}BET}$ (m^2/g)	$V_{N2\text{-}Ex}$(cm^3/g)[(a)]	$V_{N2\text{-}DR}$(cm^3/g)	$V_{CO2\text{-}DR}$(cm^3/g)	($V_{N2\text{-}DR}$ - $V_{CO2\text{-}DR}$)(cm^3/g)
G-180ºC	1766	0.94	0.79	0.50	0.29
G-240ºC	2210	1.21	0.90	0.54	0.36
G-280ºC	1379	0.73	0.66	0.60	0.06

(a) Calculated from the experimental isotherm

Table 2 includes the differences between the micropore volume calculated from N_2 and CO_2 data, showing that in the case of the sample G-280ºC the difference is very low, while for the sample G-180ºC and specially for G-240ºC the differences are higher. These results indicate that sample G-280ºC presents a very narrow micropore size distribution (MPSD), as it has been also seen from the sharp knee of its N_2 adsorption isotherms. In other words, this sample generates prevalently micropores (majorly narrow micropores). On the other hand, G-

180°C and especially G-240°C have the tendency to generate ACs with a broader PSD. The same conclusion is obtained by the NLDFT PSDs, derived from the CO_2 isotherms (Fig. 3b). Even in the lower micropore range (pore width < 1.0 nm), the PSD of G-280°C is shifted towards smaller pore widths than in the case of G-180°C and G-240°C.

As a summary, G-240°C is the sample characterised by the highest porosity development, since it shows the largest total pore volume and surface area (Table 2). At the same time, it has the widest PSD, as indicated by the large difference between its total micropore volume (i.e. $V_{N2\text{-}DR}$) and narrow micropore volume (i.e $V_{CO2\text{-}DR}$) values. The PSD of G-180°C follows very similar trends to the one of G-240°C. However the extent of porosity development for the former sample is smaller, as indicated by its lower total pore volume and surface area. G-280°C is the case when KOH chemical activation is the least effective. This sample shows the lowest pore volume and surface area. Furthermore, its PSD is much narrower than in the other two samples.

3.1.3. Porosity analysis of ACs produced from cellulose and rye straw derived HTC carbon

Using the same analysis framework than that used for glucose derived HTC carbon, the effects of KOH chemical activation on cellulose and rye straw derived HTC carbons can be effectively analysed and compared to the glucose case (Table 3 and Fig. 4 and 5).

Table 3: Calculated surface area (S) and pore volume (V) using different theories (subscript) on either N_2 or CO_2 isotherms for C-200ºC, C-240ºC, C-280ºC, RS-240ºC and RS 280ºC

Sample	$S_{N2\text{-}BET}$ (m^2/g)	$V_{N2\text{-}Ex}$(cm^3/g)[(a)]	$V_{N2\text{-}DR}$(cm^3/g)	$V_{CO2\text{-}DR}$(cm^3/g)	($V_{N2\text{-}DR}$ - $V_{CO2\text{-}DR}$)(cm^3/g)
C-200ºC	1642	0.95	0.78	0.52	0.26
C-240ºC	2250	1.26	0.90	0.56	0.34
C-280ºC	891	0.50	0.45	0.40	0.05
RS-240ºC	2200	1.11	0.92	0.65	0.27
RS-280ºC	1708	0.95	0.82	0.62	0.20

[(a)]Calculated from the experimental isotherm

The porosity analysis for the chemical activation of cellulose derived HTC carbons (C-200ºC, C240ºC and C-280ºC) show very similar trends to the ones observed for glucose. The highest porosity development is observed for the sample synthesised at 240°C (C-240°C), as indicated by its highest surface area and total pore volume values (Table 3). C-200°C and C-240°C show very similar PSDs, as deduced from the high differences between the micropore volume calculated from N_2 and CO_2 data, and also as shown in the PSDs (Fig. 4).On the other hand, the sample synthesised at 280°C (C-280ºC) shows the lowest surface area and total pore volume, indicating a lower extent of activation. Furthermore, as it was also observed for G-280ºC, its PSD is mostly characterised by narrow micropores (see the very low difference between the micropore volume calculated from N_2 and CO_2 data).

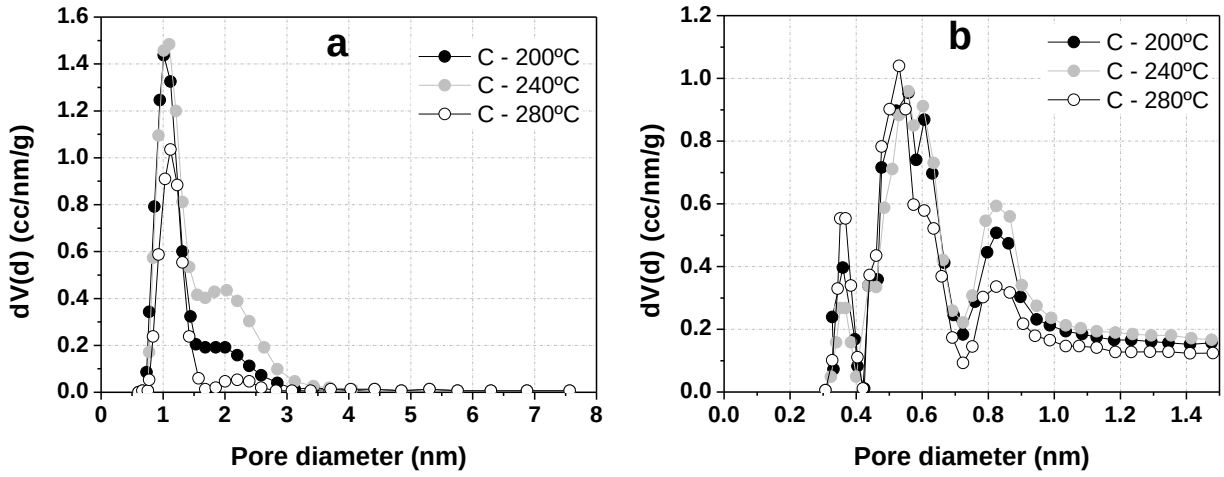

Figure 4: a) N_2 adsorption QSDFT pore size distribution and b) CO_2 NLDFT pore size distribution of C-200°C, C-240°C and C-280°C ACs.

In the case of rye straw derived HTC carbons (RS-240ºC, RS-280ºC), KOH chemical activation also generates high surface area and total pore volume ACs (Table 3). The sample synthesised at 240°C has higher porosity development than that prepared at 280 ºC. Furthermore, as indicated by its relatively high surface area and total pore volume, the sample synthesised at 280°C does not exhibit such a reduced extent of activation as for the other two carbon precursors. These dissimilarities can be explained by taking into account the more

heterogeneous composition and structure of rye straw (i.e. lignin presence and fibrous structure), which may still mildly affect the activation process, regardless of the HTC pre-treatment.

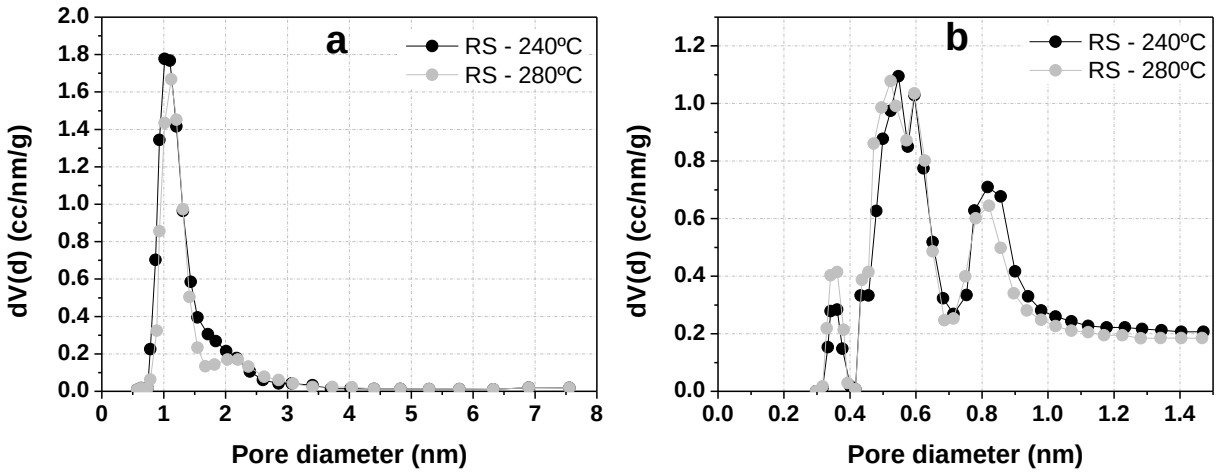

Figure 5: a) N_2 adsorption QSDFT pore size distribution and b) CO_2 NLDFT pore size distribution of RS-240^{o}C and RS–280^{o}C ACs.

Overall, this analysis highlights that the HTC temperature extensively affects the porosity of the derived ACs. HTC carbons, synthesised at higher temperatures (e.g. 280^{o}C), generate ACs with a lower porosity development and narrower PSDs, whilst the ones, produced at 180-240^{o}C, upon KOH activation, develop a greater porosity characterized by a wider PSD. These trends can be explained by taking into account the dependence of the chemical structure of HTC carbons upon the synthesis temperature [38]. Based on a 13C-Solid state NMR study, we have recently described the differences in the chemical structure of HTC carbons depending on the precursor (glucose vs. cellulose vs. lignocellulosic biomass rye straw) as well as depending on the HTC temperature [38]. Glucose can form HTC at 180°C via a polyfuranic intermediate structure. Further increase in the HTC temperature leads to aromatization and reduction in the aliphatic, functional and furanic groups. Cellulose and rye straw on the other hand, form HTC only above 200°C directly with a more aromatic structure, without going through the polyfuranic structure. All these structural differences in HTC

materials depending on the hydrothermal carbonization temperature and the type of precursors can be correlated with the different pore characteristics resulting upon chemical activation into hydrothermal carbons. More severe HTC processing conditions (i.e. higher temperatures) generate HTC carbons with a higher degree of aromatisation, resulting into enhanced chemical stability and structural order. As observed for the hydroxide activation of several coals, both features are detrimental to the reactivity of the carbon substrate, leading to a reduced porosity development [39]. These aspects were also observed in our previous work [23], where it was compared the KOH activation of anthracite with the KOH activation of the pyrolysed anthracite (at 1000 ºC). It was observed that pyrolysis prior to activation decreased the porosity development. Moreover, when the anthracite was pyrolyzed up to 1800 ºC prior to activation, no porosity development by chemical activation was possible for KOH.

3.2. CO_2 and CH_4 storage using the HTC-derived ACs

To evaluate the effectiveness of the HTC derived ACs as CO_2 adsorbents, CO_2 adsorption isotherms at 0ºC and 25 ºC were carried out up to 30 bar and 40 bar, respectively, for three activated HTC carbons prepared from the three different precursors at the same carbonization temperature (240 ºC) (see Fig. 6 and Fig.7). As it was described in our previous study [40], the shape of these isotherms provides information about the porosity of the samples.

All CO_2 adsorption isotherms are of type I, characteristic of microporous materials. The activated carbon prepared from Rye Straw presents a sharper knee than those prepared from Glucose and Cellulose, suggesting that the former presents a narrower micropore size distribution than the glucose and cellulose derived activated carbons. The CO_2 uptakes (around 25 mmol g^{-1}) at 30 bar and 0ºC for HTC derived ACs are comparable to those obtained with superactivated carbons prepared by KOH activation of anthracites with similar micropore volume [40]. In the case of adsorption at room temperature (25ºC; Fig. 7), these materials adsorb up to 2.80 mmol g^{-1} CO_2 at 1 bar, and almost 20 mmol g^{-1} at 40 bar. The

measured CO_2 uptake at 25 ºC and 30 bar for the three HTC derived ACs are plotted versus the micropore volume in Figure 8, together with the values corresponding to activated carbons prepared in our laboratory by chemical activation with hydroxides of coals of different rank. The performance of the HTC derived ACs are similar to ACs with similar development of porosity, and also is comparable with related porous solids found in the literature [41] and with other type of porous materials, such as microporous organic polymers [42].

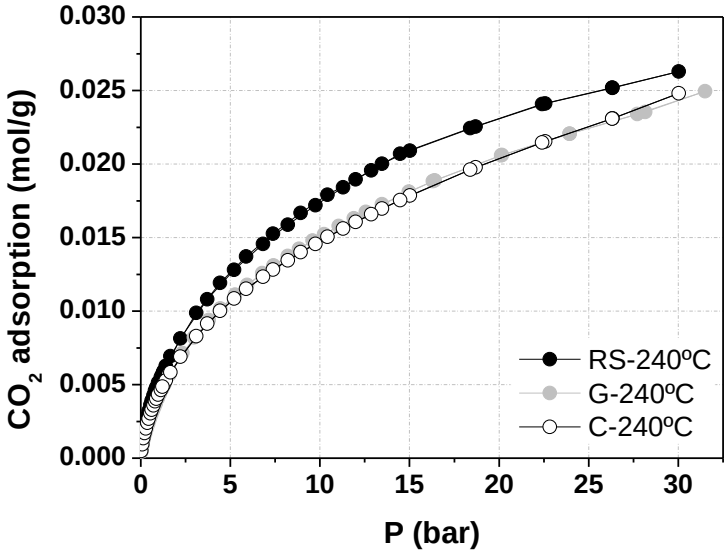

Figure 6. CO_2 adsorption isotherms at 0ºC and up to 30 bar for three activated hydrochars prepared from Glucose, Cellulose and Rye Straw on gravimetric basis.

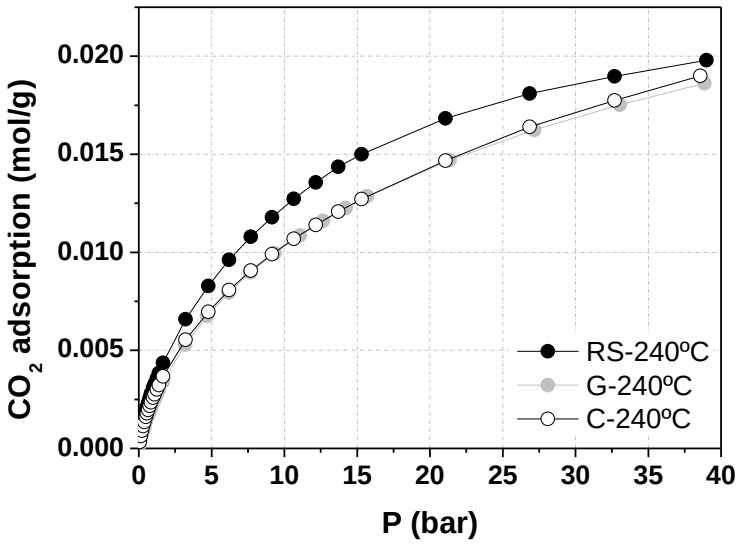

Figure 7. CO_2 adsorption isotherms at 25 ºC and up to 40 bar for three activated hydrochars prepared from Glucose, Cellulose and Rye Straw on gravimetric basis.

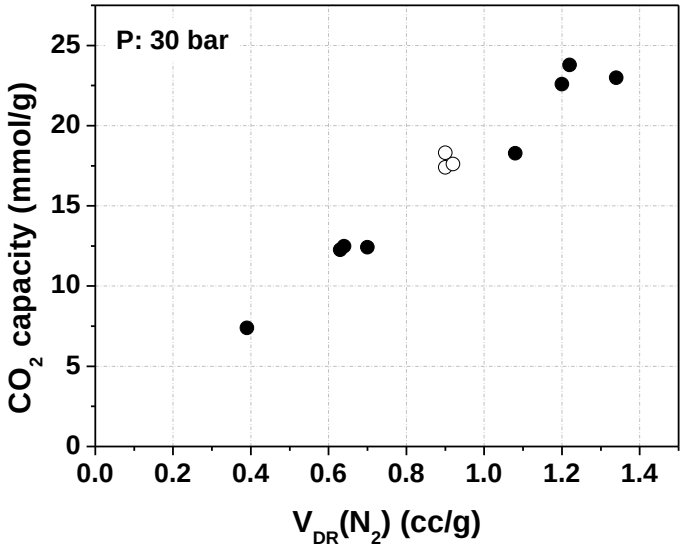

Figure 8. CO_2 uptake (at 25 ºC and 30 bar) versus the total micropore volume corresponding to: the three HTC derived ACs obtained in the present study (empty symbols) and activated carbons prepared in our laboratory by KOH activation of other precursors (filled symbols).

The same three HTC derived ACs tested as CO_2 adsorbents were also studied as materials for high pressure CH_4 storage. Figure 9 presents the methane adsorption isotherms on a

gravimetric basis for these samples, which have very similar methane adsorption capacities, since, as just shown, the porosity development for all of them is quite similar. It is well established that CH_4 adsorption on porous materials at these conditions (room temperature and high pressures) takes place in micropores [43-45]. In this sense, the results obtained in a previous study with activated carbon fibres and powder activated carbons, covering a wide range of micropore volume (up to 1.5 $cm^3\ g^{-1}$) [44], pointed out that a general trend exists for this type of materials: the higher the micropore volume, the higher the methane adsorption capacity. It was concluded that, for samples with relatively narrow micropore size distribution, the total micropore volume -$V_{DR}(N_2)$- obtained from DR equation could be a good indicator of the methane capacity. The preliminary study carried out with HTC derived ACs, has given CH_4 uptakes as high as 9 mmol CH_4/g_{sample} at 40 bar , being values comparable with activated carbons with similar $V_{DR}(N_2)$ obtained from other precursors [44], as shown in Figure 10.

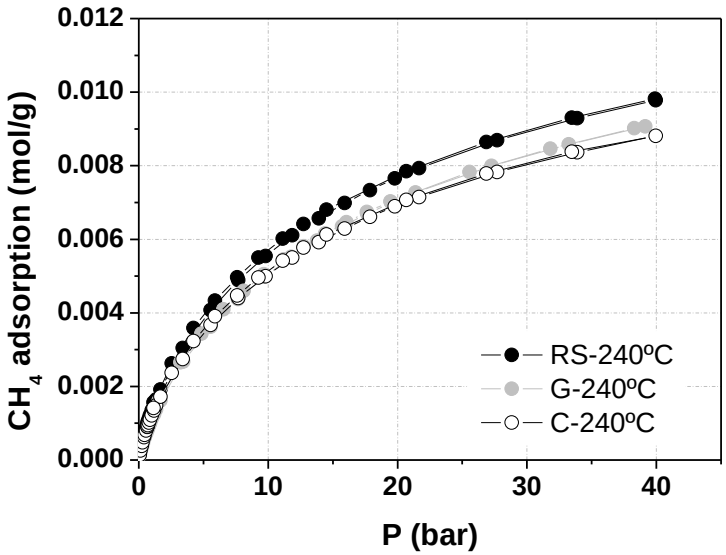

Figure 9. CH_4 adsorption isotherms at 25 ºC and up to 40 bar for three activated hydrochars prepared from Cellulose, Glucose and Rye Straw on gravimetric basis.

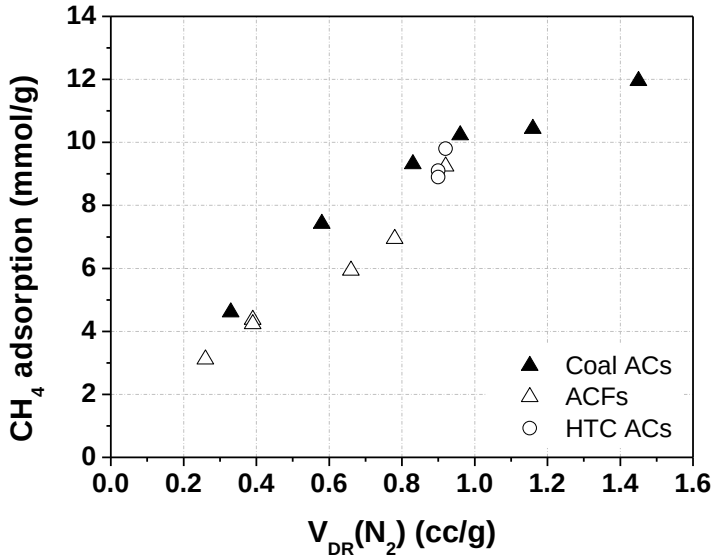

Figure 10. Methane adsorption capacity (at 25 ºC and 40 bar) versus the micropore volume corresponding to KOH anthracite derived ACs (coal ACs) (from [43]), activated carbon fibres (ACFs) (from [44]), and the three HTC derived ACs obtained in the present study.

In addition to micropore volume and micropore size distribution, methane storage in volumetric basis, also depends on another important parameter, i.e. the density of the material. Table 4 contains the values corresponding to the "tap density" and the "packing density" obtained as explained in Experimental Section for the three activated hydrochars. In our previous work carried out with activated carbons (obtained by KOH activation of an anthracite), it was clearly shown that, for both type of densities (tap and packing), a general trend was observed: the higher the porosity development of the materials, the lower the density, following a linear trend [36]. Comparing with those results, it can be said that the densities of the HTC carbons prepared in the present study are lower than activated carbons from anthracite with similar micropore volume (e.g packing density of an anthracite based activated carbon with a $V_{DR}(N_2)$ of 0.92 cm^3/g is 0.62 g/cm^3 [36]). Table 4 also contains the volumetric methane uptake calculated from the methane isotherms and using the packing densities.

Table 4. Tap and Packing Densities of Three Activated Samples. Calculated methane uptake (volume of methane adsorbed per volume of sample: V/V)

Sample	Tap density (g/cm^3)	Packing density (g/cm^3)	CH4 uptake (V/V)
RS-240 ºC	0.13	0.43	105
C-240 ºC	0.12	0.39	86
G-240 ºC	0.11	0.38	86

These excellent preliminary results could be further improved by tailoring the PSD of the ACs to the optimum pore width value for methane adsorption (ca. 0.8-1.1 nm) [43-45]. Such specific material pore size features could be achieved by tuning the KOH activation process parameters and the chemical structure of the parent HTC carbon.

The synthesis strategy presented in this work (HTC followed by KOH activation) allowed converting a low value lignocellulosic biomass into a functional carbon material with high performance in gas storage applications. In the literature, the use of other porous materials, such us metal–organic frameworks (MOFs) [46], organic polymer networks [47] and templated nanocarbons [48], for energy related applications have been studied. A common property of those materials is the high production cost and poor mass-production. Moreover, in the case of MOF and nanoporous organic polymer networks, they present low chemical and structural stabilities, as it has been demonstrated for MOFs elsewhere [49].

4. Conclusions

The present work highlights that HTC carbons are excellent precursors for the synthesis of ACs via KOH chemical activation. Regardless of the parent biomass (i.e. glucose, cellulose or rye straw), highly microporous ACs could be generated. The HTC temperature was found to be an extremely influential parameter affecting the porosity development and PSDs of the ACs. Tuning of the MPSD of the ACs was achived by modification of the HTC temperature.

The use of higher HTC temperatures (i.e. 280^{o}C) led to lower porosity development, but to a narrower PSD mostly composed of micropores. On the other hand, KOH chemical activation of HTC carbons, synthesised at lower temperatures (i.e. 180 - 240^{o}C), produced ACs with higher total pore volume and broader PSDs.

Preliminary testing of the synthesised ACs as adsorbents for either CO_2 capture (0^{o} C and 25 ^{o}C) or high pressure CH_4 storage, yielded very promising results. The measured uptakes of both adsorbates were comparable to top-performing and commercially available adsorbents usually employed for these end-applications. Further improvements of the synthesised ACs performance could certainly be achieved by optimising the activation and HTC synthesis parameters, in such a way as to tailor their PSDs to the adsorbate.

Overall, the present work shows the effectiveness of this synthesis strategy in tuning the PSD of ACs and converting a low value lignocellulosic biomass into a functional carbon material with high performance in gas storage applications.

Acknowledgements

MMT and CF would like to thank the Max-Planck Society for financial support. DLC, DST, JPML and DCA would like to thank the Spanish MINECO, Generalitat Valenciana and FEDER (Projects CTQ2012-31762 and PROMETEO/2009/047) for financial support. DST. thanks MICCIN (BES-2010-035238). The authors thank Ms. Silvia Pirok (Max Planck Institute of Colloids and Interfaces, Golm, Germany) for the elemental analysis results.

References

[1] Baccile N, Laurent G, Babonneau F, Fayon F, Titirici MM, Antonietti M. Structural characterization of hydrotermal carbon spheres by advanced solid-state MAS ^{13}C NMR Investigation. J. Phys. Chem. C 2009 ;113(22):9644-9654.

[2] Falco C, Perez Caballero F, Babonneau F, Gervais C, Laurent G, Titirici MM, Baccile N, Hydrothermal Carbon from Biomass: Structural Differences between Hydrothermal and Pyrolyzed Carbons via 13C Solid State NMR, Langmuir, 2011,27 (23):14460-14471

[3] Falco C, Sieben J M, Brun N, Sevilla M, van der Mauelen T, Morallón E, Cazorla-Amorós D, Titirici M M, Hydrothermal Carbons From Hemicellulose-Derived Aqueous Hydrolysis Products As Electrode Materials For Supercapacitors, ChemSusChem, 2013, 6, 374-382.

[4] Titirici MM, Antonietti M. Chemistry and materials options of sustainable carbon materials made by hydrothermal carbonization. Chem. Soc. Rev. 2010(39):103-116.

[5] Bergius F. Beiträge zur Theorie der Kohleentstehung, Die Naturwissenschaften. 1928(16):1-10.

[6] Titirici MM, White RJ, Falco C, Sevilla M. Black perspectives for a green future: hydrothermal carbons for environment protection and energy storage. Energy Environ. Sci. 2012(5): 6796-6822.

[7] Angyal SJ. In Glycoscience: epimerisation, isomerisation and rearrangement reactions of carbohydrates. Springer-Verlag: Berlin. 2001:1-14.

[8] Patil SKR, Lund CFR. Formation and growth of humins via aldol addition and condensation during acid-catalyzed conversion of 5-Hydroxymethylfurfural. Energy Fuels 2011(25):4745-4755.

[9] Dutta S, De S, Saha B. A Brief Summary of the Synthesis of Polyester Building-Block Chemicals and Biofuels from 5-Hydroxymethylfurfural. Chempluschem 2012(77):259-272.

[10] Yu L, Falco C, Weber J, White R, Howe J Y, Titirici MM, Carbohydrate Derived Hydrothermal Carbons: A Thorough Characterization Study, Langmuir 2012 (28): 12373-12383

[11] Kubo S, Tan I, White RJ, Antonietti M, Titirici MM. Template synthesis of carbonaceous tubular nanostructures with tunable surface properties. Chem. Mat. 2010(22):6590-6597.

[12] Kubo S, Demir-Cakan Zhao L, White RJ, Titirici MM. Porous carbohydrate-based materials via hard templating. ChemSusChem 2010(3):188-194.

[13] White RJ, Tauer K, Antonietti M, Titirici MM. Functional hollow carbon nanospheres via latex templating, J. Am. Chem. Soc. 2010(132):17360-17363.

[14] Bansal RC, Donnet JB, Stoeckli F. Active Carbon. Marcel Dekker: New York. 1988.

[15] Muñoz-Guillena MJ, Illán-Gómez MJ, Martín-Martínez A and Salinas-Martínez de Lecea C, Activated carbons from Spanish coals. 1. Two-stage CO2 activation, Energy and Fuels 1992 (6): 9-15.

[16] Evans MJB, Halliop E, MacDonald JAF. The production of chemically-activated carbon. Carbon 1999 (37): 269-274.

[17] Perrin A, Celzard A, Albiniak A, Kaczmarczyk J, Marêché JF, Furdin G. NaOH activation of anthracites: effect of temperature on pore textures and methane storage ability. Carbon 2004 (42): 2855-2866.

[18] Lozano-Castello D, Lillo-Rodenas MA, Cazorla-Amoros D, Linares-Solano A. Preparation of activated carbons from Spanish anthracite: I. Activation by KOH. Carbon 2001(39):741-749.

[19] Lillo-Rodenas MA, Lozano-Castello D, Cazorla-Amoros D, Linares-Solano A. Preparation of activated carbons from Spanish anthracite: II. Activation by NaOH. Carbon 2001(39):751-759.

[20] Lozano-Castello D, Calo JM, Cazorla-Amoros D, Linares-Solano A. Carbon activation with KOH as explored by temperature programmed techniques, and the effects of hydrogen Carbon 2007(45):2529-2536.

[21] Khezami L, Chetouani A, Taouk B, Capart R. Production and characterization of activated carbon from wood components in powder: Cellulose, lignin, xylan. Powder Technol. 2005(157):48-56.

[22] Basta AH, Fierro V, El-Saied H, Celzard A. 2-steps KOH activation of rice straw: An efficient method for preparing high-performance activated carbons. Bioresource Technology 2009(100): 3941-3947.

[23] Lillo-RodenasMA, Marco-LozarJP, Cazorla-Amoros D,Linares-Solano A, Activated carbons prepared by pyrolysis of mixtures of carbon precursor/alkaline hydroxide,J. Anal. Appl. Pyrolysis, 2007(80): 166–174.

[24] Wei L, Sevilla M, Fuertes AB, Mokaya R, Yushin G. Hydrothermal carbonisation of abundant renewable natural organic chemicals for high-performance supercapacitor electrodes. Adv. Energy Mater. 2011(1):356-361.

[25] Sevilla M, Fuertes AB, Mokaya R. High density hydrogen storage in superactivated carbons from hydrothermally carbonized renewable organic materials. Energy Environ. Sci. 2011(4):1400-1410.

[26] Sevilla M, Fuertes AB. Sustainable porous carbons with a superior performance for CO_2 capture. Energy Environ. Sci. 2011(4):1765-1771.

[27] Zhao L, Baccile N, Gross S, Zhang Y, Wei W, Sun Y, Antonietti M, Titirici MM. Sustainable nitrogen-doped carbonaceous materials from biomass derivatives. Carbon 2010(48):3778-3787.

[28] Zhao L, Fan LZ, Zhou MQ, Guan H, Qiao S, Antonietti M, TitiriciMM. Nitrogen-containing hydrothermal carbons with superior performance in supercapacitors. Adv. Mater. 2010(22):5202-5206.

[29] Zhang B, Ren J, Gu X, Liu X, Li C, Shi B, Guo Y, Guo Y, Lu G, Wang Y. A method for the preparation of activated carbon based carbon/carbonaceous composites with controllable surface functionality. J. Porous Mat. 2011(18) 743-750.

[30] Zhang WL, Tao HX, Zhang BH, Ren JW, Lu GZ, Wang YQ. One-post synthesis of carbonaceous monolith with surface sulfonic groups and its carbonisation/activation. Carbon 2011(49) 1811-1820.

[31] Román S, Valente Nabais JM, Ledesma B, González JF, Laginhas C, Titirici MM. Production of low-cost adsorbents with tunable surface chemistry by conjunction of hydrothermal carbonization and activation processes. Micropor. Mesopor. Mat. 2013(165):127-133.

[32] Walton KS, Snurr RQ. Applicability of the BET Method for determining surface areas of microporous metal−organic frameworks. J. Am. Chem. Soc. 2007(129):8552-8556.

[33] Cazorla-Amoros D, Alcañiz-Monge J, Linares-Solano A, Characterization of activated carbon fibers by CO_2 adsorption, Langmuir 1996(12): 2820–2824.

[34] Cazorla-Amoros D, Alcañiz-Monge J, de la Casa-Lillo MA, Linares-Solano A. CO_2 as an adsorptive to characterize carbon molecular sieves and activated carbons. Langmuir 1998(14): 4589–4596.

[35] Lozano-Castello D, Cazorla-Amoros D, Linares-Solano A. Usefulness of CO_2 adsorption at 273 K for the characterization of porous carbons. Carbon 2004 (42): 1233-1242.

[36] Jorda-Beneyto M, Lozano-Castello D, Suarez-García F, Cazorla-Amoros D, Linares-Solano A. Advanced activated carbon monoliths and activated carbons for hydrogen storage. Micropor. Mesopor. Mater. 2008(112):235–242.

[37] Figueiredo JL, Pereira MFR, Freitas MMA, Orfao JJM. Modification of the surface chemistry of activated carbons. Carbon 1999(37):1379-1389.

[38] Falco C, Baccile N, Titirici MM, Morphological and structural differences between glucose, cellulose and lignocellulosic biomass derived hydrothermal carbons.Green Chem. 2011(13):3273-3281.

[39] Lillo-Rodenas MA, Juan-Juan J, Cazorla-Amoros D, Linares-Solano A. About reactions occurring during chemical activation with hydroxides. Carbon 2004(42):1371-1375.

[40] Lozano-Castello D, Cazorla-Amoros D, Linares-Solano A, Quinn DF. Micropore size distributions of activated carbons and carbon molecular sieves assessed by high-pressure methane and carbon dioxide adsorption isotherms. J Phys. Chem. B 2002(106):9372-9379.

[41] Marco-Lozar JP, Juan-Juan J, Suárez-García F, Cazorla-Amorós D, Linares-Solano A. MOF-5 and activated carbons as adsorbents for gas storage. Int. J. Hydrogen Energ. 2012; 37(3):2370–2381.

[42] Dawson R, Stöckel E, Holst JR, Adams DJ, Cooper AI. Microporous organic polymers for carbon dioxide capture. Energy Environ. Sci. 2011(4):4239-4245.

[43] Lozano-Castello D, Cazorla-Amoros D, Linares-Solano A, Quinn DF, Influence of pore size distribution on methane storage at relatively low pressure: preparation of acivated carbon with optimum pore size. Carbon 2002(40):989-1002.

[44] Lozano-Castello D, Alcañiz-Monge J, de la Casa-Lillo MA, Cazorla-Amorós D, Linares-Solano A. Advances in the study of methane storage in porous carbonaceous materials. Fuel 2002(81):1777- 1803.

[45] Alcañiz-Monge J, Lozano-Castello D, Cazorla-Amorós D, Linares-Solano A. Fundamentals of methane adsorption in microporous carbons. Micropor. Mesopor. Mater. 2009(124):110-116.

[46] Ma S, Zhou HC. Gas storage in porous metal–organic frameworks for clean energy applications Chemical Communication 2010 (46): 44-53

[47] Dawson R, Cooper AI, Adams DJ. Nanoporous organic polymer networks. Progress in Polymer Science 2012 (37): 530-563.

[48] Nishihara H, Kyotani T. Templated Nanocarbons for Energy Storage. Advanced Materials 2012 (24): 4473-4498.

[49] Marco-Lozar, JP, Juan-Juan J, Suárez-García F, Cazorla-Amorós D, Linares-Solano A. MOF-5 and activated carbons as adsorbents for gas storage. International Journal of Hydrogen Energy 2012 (37): 2370-2381.

Figure captions

Figure 1. SEM micrographs of the hydrothermal carbon before chemical activation: (a) HTC from glucose at 240°C; (b) HTC from cellulose at 240°C; (c) HTC from rye straw at 240°C. And after chemical activation: b) glucose (G–240ºC), d) cellulose (C–240ºC) and f) rye straw (RS–240ºC).

Figure 2. a) N_2 adsorption isotherms, b) N_2 adsorption QSDFT PSD of ACs (G-180^{o}C, G-240^{o}C, G-280^{o}C)

Figure 3. a) CO_2 (0 ºC) isotherms and b) NLDFT PSD of ACs (G-180^{o}C, G-240^{o}C, G-280^{o}C)

Figure 4. a) N_2 adsorption QSDFT pore size distribution and b) CO_2 NLDFT pore size distribution of C-200^{o}C, C-240^{o}C and C-280^{o}C ACs.

Figure 5. a) N_2 adsorption QSDFT pore size distribution and b) CO_2 NLDFT pore size distribution of RS - 240^{o}C and RS – 280^{o}C ACs.

Figure 6. CO_2 adsorption isotherms at 0ºC and up to 30 bar for three activated hydrochars prepared from Glucose, Cellulose and Rye Straw on gravimetric basis.

Figure 7. CO_2 adsorption isotherms at 25 ºC and up to 40 bar for three activated hydrochars prepared from Glucose, Cellulose and Rye Straw on gravimetric basis.

Figure 8. CO_2 uptake (at 25 ºC and 30 bar) versus micropore volume corresponding to: the three HTC derived ACs obtained in the present study (empty symbols)and activated carbons prepared in our laboratory by KOH activation of other precursors (filled symbols).

Figure 9. CH_4 adsorption isotherms at 25 ºC and up to 40 bar for three activated hydrochars prepared from Cellulose, Glucose and Rye Straw on gravimetric basis.

Figure 10. Methane adsorption capacity (at 25 ºC and 40 bar) versus the micropore volume corresponding to KOH anthracite derived ACs (coal ACs) (from [43]), activated carbon fibres (ACFs) (from [44]), and the three HTC derived ACs obtained in the present study.

Table captions

Table 1. EA of HTC carbon derived ACs and pyrolysed HTC carbon

Table 2. Calculated surface area (S) and pore volume (V) using different theories (subscript) on either N_2 or CO_2 isotherms for G-180^{o}C, G-240^{o}C, G-280^{o}C

Table 3. Calculated surface area (S) and pore volume (V) using different theories (subscript) on either N_2 or CO_2 isotherms for C-200ºC, C-240ºC, C-280ºC, RS-240ºC and RS 280ºC

Table 4. Tap and Packing Densities of Three Activated Samples. Calculated methane uptake (volume of methane adsorbed per volume of sample: V/V)

Table 1: EA of HTC carbon derived ACs and pyrolysed HTC carbon

	Elemental Composition (wt%)			
Sample	**C%**	**H%**	**O%**	**N%**
HTC carbon derived ACs[(a)]	85.0-88.0	1.5-2.1	10.1-12.8	0.1-0.4
HTC-Δ750[(b)]	94.0	1.7	4.2	0.1

[(a)] The EA of each AC can be found in the supporting information (Table S1)
[(b)] HTC carbon pyrolysed at 750 ºC

Table 2. Calculated surface area (S) and pore volume (V) using different theories (subscript) on either N_2 or CO_2 isotherms for G-180^oC, G-240^oC, G-280^oC

Sample	$S_{N2\text{-}BET}$ (m^2/g)	$V_{N2\text{-}Ex}$(cm^3/g)[(a)]	$V_{N2\text{-}DR}$(cm^3/g)	$V_{CO2\text{-}DR}$(cm^3/g)	($V_{N2\text{-}DR}$ - $V_{CO2\text{-}DR}$)(cm^3/g)
G-180ºC	1766	0.94	0.79	0.50	0.29
G-240ºC	2210	1.21	0.90	0.54	0.36
G-280ºC	1379	0.73	0.66	0.60	0.06

(a) Calculated from the experimental isotherm

Table 3. Calculated surface area (S) and pore volume (V) using different theories (subscript) on either N_2 or CO_2 isotherms for C-200ºC, C-240ºC, C-280ºC, RS-240ºC and RS 280ºC

Sample	$S_{N2\text{-}BET}$ (m^2/g)	$V_{N2\text{-}Ex}$ (cm^3/g)[(a)]	$V_{N2\text{-}DR}$ (cm^3/g)	$V_{CO2\text{-}DR}$ (cm^3/g)	$(V_{N2\text{-}DR} - V_{CO2\text{-}DR})$ (cm^3/g)
C-200ºC	1642	0.95	0.78	0.52	0.26
C-240ºC	2250	1.26	0.90	0.56	0.34
C-280ºC	891	0.50	0.45	0.40	0.05
RS-240ºC	2200	1.11	0.92	0.65	0.27
RS-280ºC	1708	0.95	0.82	0.62	0.20

[(a)]Calculated from the experimental isotherm

Table 4

Table 4. Tap and Packing Densities of Three Activated Samples. Calculated methane uptake (volume of methane adsorbed per volume of sample: V/V)

Sample	Tap density (g/cm^3)	Packing density (g/cm^3)	CH4 uptake (V/V)
RS-240 ºC	0.13	0.43	105
C-240 ºC	0.12	0.39	86
G-240 ºC	0.11	0.38	86

Figure 1

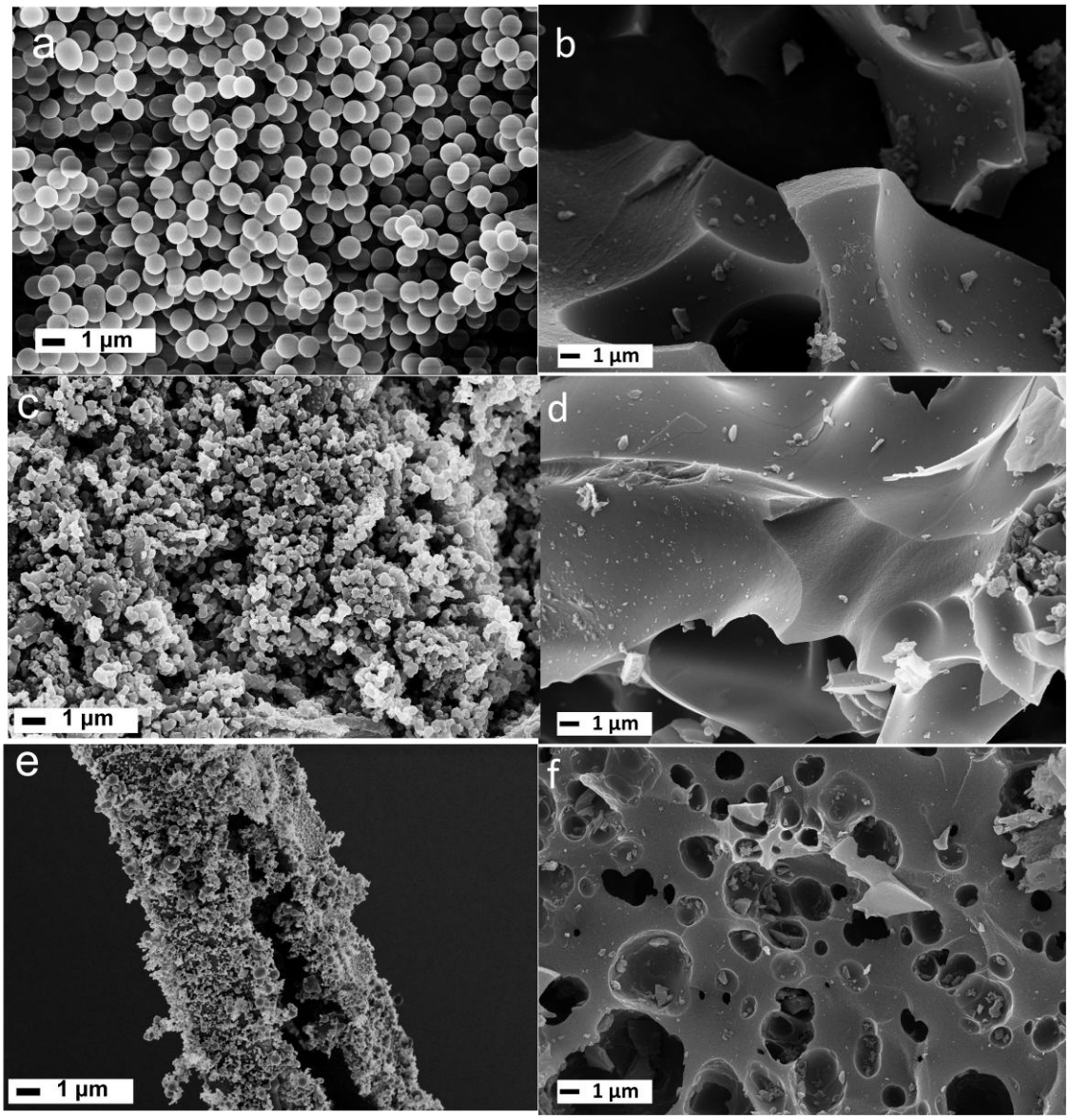

Figure 1: SEM micrographs of the hydrothermal carbon before chemical activation: (a) HTC from glucose at 240°C; (b) HTC from cellulose at 240°C; (c) HTC from rye straw at 240°C. And after chemical activation: b) glucose (G–240ºC), d) cellulose (C–240ºC) and f) rye straw (RS–240ºC).

Figure 2

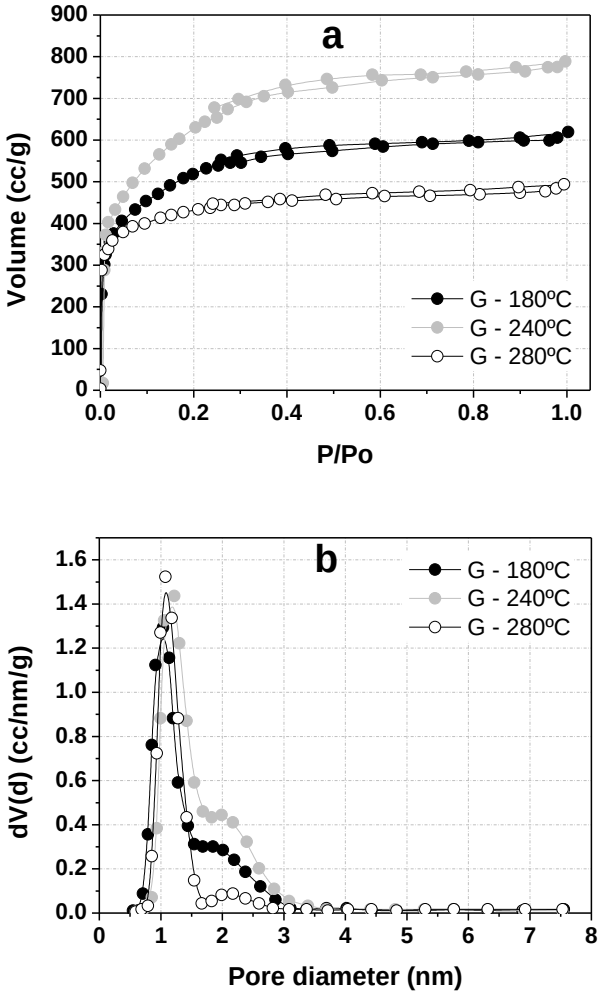

Figure 2. a) N_2 adsorption isotherms, b) N_2 adsorption QSDFT PSD of ACs (G-180^{o}C, G-240^{o}C, G-280^{o}C)

Figure 3

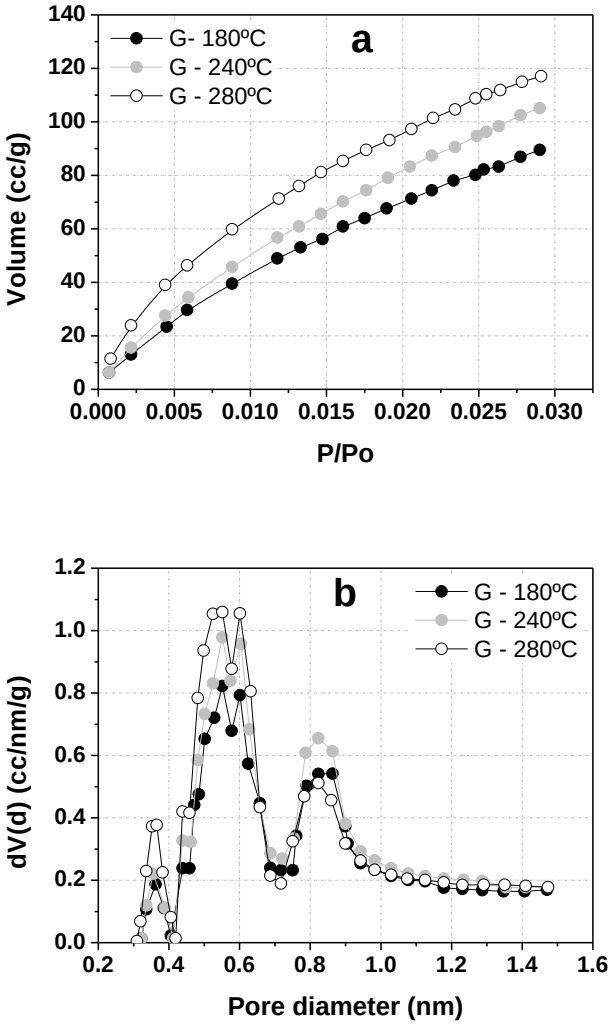

Figure 3. a) CO_2 (273 K) isotherms and b) NLDFT PSD of ACs (G-180^{o}C, G-240^{o}C, G-280^{o}C)

Figure 4

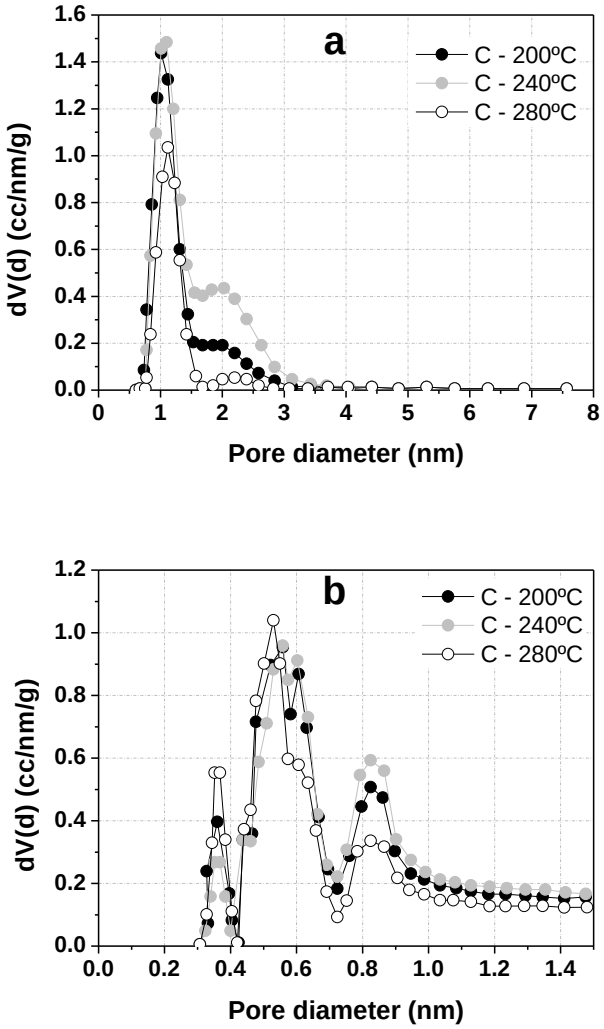

Figure 4. a) N_2 adsorption QSDFT pore size distribution and b) CO_2 NLDFT pore size distribution of C-200^{o}C, C-240^{o}C and C-280^{o}C ACs.

Figure 5

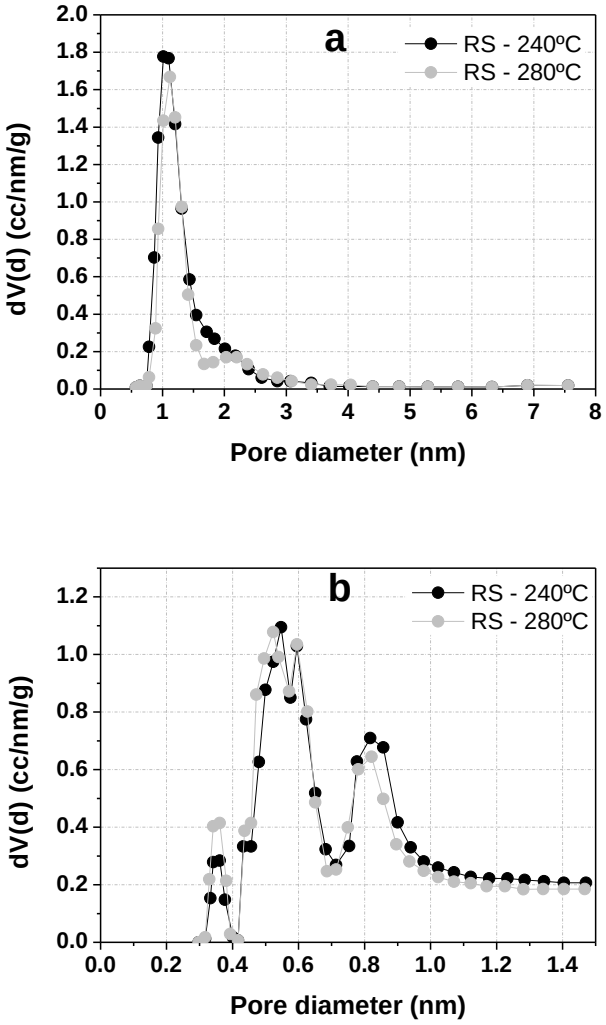

Figure 5. a) N_2 adsorption QSDFT pore size distribution and b) CO_2 NLDFT pore size distribution of RS - 240^{o}C and RS – 280^{o}C ACs.

Figure 6

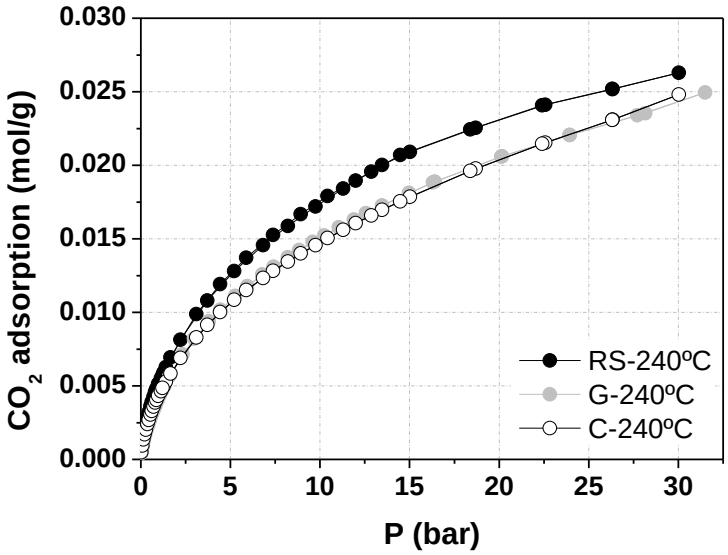

Figure 6. CO_2 adsorption isotherms at 273 K and up to 30 bar for three activated hydrochars prepared from Glucose, Cellulose and Rye Straw on gravimetric basis.

Figure 7

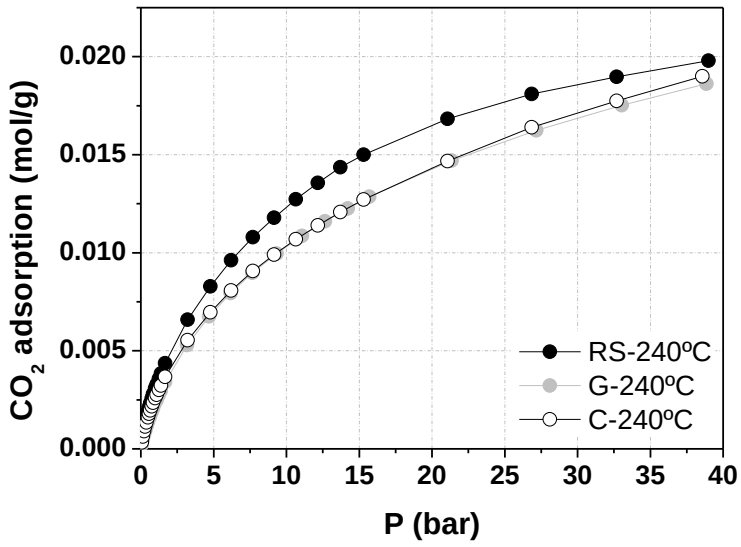

Figure 7. CO_2 adsorption isotherms at 298 K and up to 40 bar for three activated hydrochars prepared from Glucose, Cellulose and Rye Straw on gravimetric basis.

Figure 8

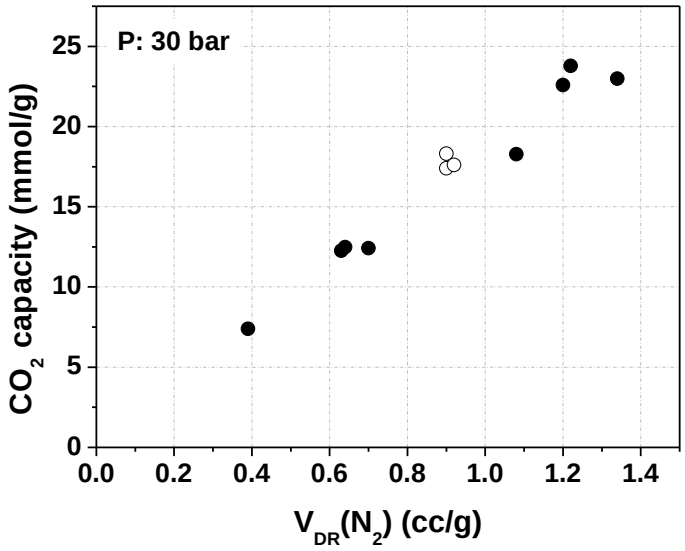

Figure 8. CO_2 uptake (at 298 K and 30 bar) versus the total micropore volume corresponding to: the three HTC derived ACs obtained in the present study (empty symbols) and activated carbons prepared in our laboratory by KOH activation of other precursors (filled symbols).

Figure 9

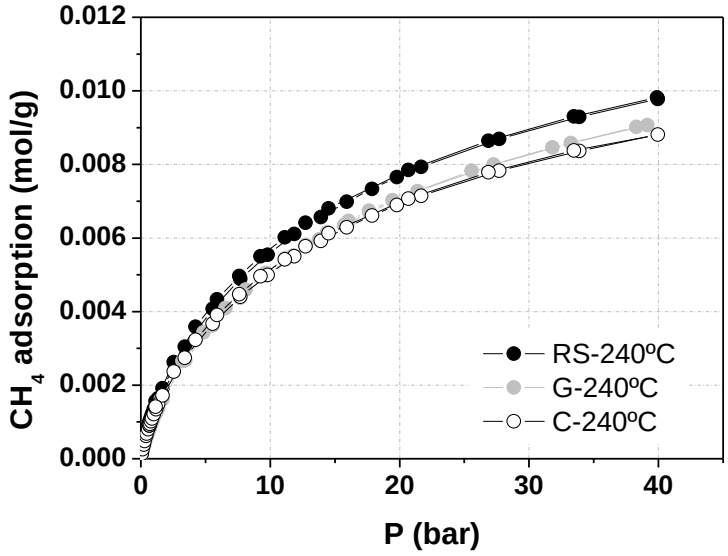

Figure 9. CH_4 adsorption isotherms at 298 K and up to 40 bar for three activated hydrochars prepared from Cellulose, Glucose and Rye Straw on gravimetric basis.

Figure 10

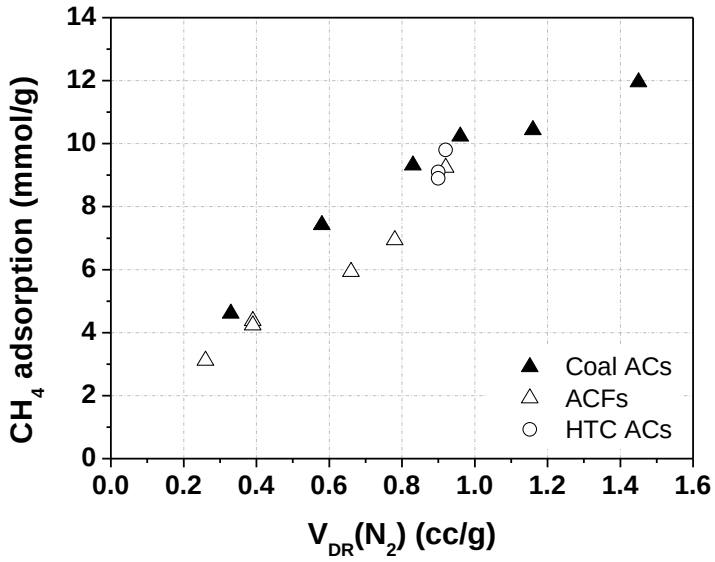

Figure 10. Methane adsorption capacity (at 298 K and 40 bar) versus the micropore volume corresponding to KOH anthracite derived ACs (coal ACs) (from [39]), activated carbon fibres (ACFs) (from [40]), and the three HTC derived ACs obtained in the present study.

Supplementary Material

Click here to download Supplementary Material: Supporting Information_revised.docx